RSC Advances

PAPER

Check for updates

Theoretical investigation on donor–acceptor interaction between a carbonyl compound and an N,N'-dioxide–Sc(III) complex†

Zhishan Su, [iD] Weiying He, Junming Wang, Yini Zuo and Changwei Hu [iD] *

Herein, metal–ligand bonding features in a chelation N,N'-dioxide–Sc(III) complex have been addressed using the DFT method at the M06/6-31+G** Level. The donor–acceptor interaction between the carbonyl substrate and Sc(III)-based catalyst is analyzed in detail by the activation strain model (ASM), energy decomposition analysis (EDA), and natural orbital for chemical valence (NOCV) calculations. The orbital interaction is the major contributor to N,N'-dioxide–[Sc(OTf)]$^{2+}$ bonding, whereas the electrostatic interaction plays a more important role than orbital interaction in the activation of a carbonyl compound in hexacoordinate N,N'-dioxide–Sc(III) complexes. The substituents in the amide group of the N,N'-dioxide ligand (L) affect the electrostatic energy as well as the orbital energy between the CH_2O and Sc(III)-based catalyst by adjusting the Lewis acidity of the metal centre. The complex with ortho-diisopropylphenyl groups in the ligand exhibits a higher reactivity towards CH_2O. Compared to OiPr, the counter ion OTf in the Sc(III)-complex enhances the Lewis acidity of the metal centre and facilitates the activation of CH_2O by promoting electron density flow from CH_2O to the metal fragment. The high catalytic performance of the N,N'-dioxide–Sc(III) complex towards PhCHO and chalcone is attributed to their good nucleophilicity that results in a more stabilizing electrostatic and orbital interaction between the N,N'-dioxide–[Sc(OTf)]$^{2+}$ complex and carbonyl substrate.

Introduction

The C_2-symmetric N,N'-dioxide (L) developed by Feng's group is a class of conformationally flexible ligands, which can be synthesized from cheap optically pure amino acids.[1] The experimental investigations indicate that these ligands can act as neutral tetradentate ligands to bind a wide variety of metal ions; this results in the formation of effective and versatile chiral metal-complex catalysts for asymmetric catalysis.[1a,b] After coordination at the metal centre, the chelating ligand is able to impose a relatively rigid environment, tuning the electron richness of metal centre and, in turn, the reactivity of the coordination complex.[2] In the catalytic processes involving N,N'-dioxide–metal complexes, the carbonyl compound is one of the most popular substrates since it can coordinate towards the metal centre in a monodentate or bidentate fashion (if possible) via oxygen atoms to form reacting species. When only one coordinating O atom is available in a carbonyl compound,

Key Laboratory of Green Chemistry and Technology, Ministry of Education, College of Chemistry, Sichuan University, Chengdu, Sichuan, 610064, P. R. China. E-mail: changweihu@scu.edu.cn

† Electronic supplementary information (ESI) available: Cartesian coordinates of all stationary points and energies; selected geometric and electronic parameters as well as results of for ETS-NOCV analysis Sc(III)-complexes. See DOI: 10.1039/c7ra12258f

another ligand, solvent or counter anion can occupy the remaining coordination site to construct an octahedral intermediate for subsequent conversion. The experimental observations and theoretical investigations indicate that the activity and selectivity of a chiral N,N'-dioxide–metal catalyst towards a carbonyl substrate depend closely on the inherent properties (such as Lewis acidity, ionic radius or coordination sphere properties) of the central metal ion as well as ligand structures (amide substituent or the amino acid backbone).[3]

The classical Dewar–Chatt–Duncanson model is generally employed to understand the metal–ligand interaction in organometallic chemistry.[4,5] For transition metal-based systems, bonding is attributed to a synergic process of ligand → metal electron donation and metal → ligand back-donation.[6] Many useful schemes, including charge decomposition analysis (CDA),[7–10] atoms in molecule (AIM),[11] block localized wave function energy decomposition (BLW-ED),[12] interaction-energy partition analysis,[13] lever electronic parameters,[14] and molecular electrostatic potential (MEP),[15] have been developed to describe this donor–acceptor interaction in metallic complexes. In addition, the results obtained from spectroscopic measurement, such as infrared stretching frequencies (e.g. Tolman electronic parameter (TEP))[7,14a–c] and NMR chemical shifts,[16] can be used as indicators to evaluate the electronic donation of the ligand, or monitor structural as well as energetic changes in complexes with different ligands. Clot and co-

workers calculated the vibrational frequency of CO in $[Ni(CO)_3L]$ complexes (L = P-donor ligands) by the B3PW91 method.[17] The better the donor ability of phosphine (R_3P) in the $[Ni(CO)_3R_3P]$ complex, the lower the $\nu(CO)$ vibration becomes as a result of back-donation from metal d orbitals into the low-lying anti-bonding π_{CO}^* orbital.[14a,17] The activation strain model (ASM)[18–20] or distortion/interaction model[21–23] combined with energy decomposition analysis (EDA)[24] provides a quantitative tool to understand the physical factors controlling the bonding energy or activation barrier in reactions. Recently, as a useful approach, a combination of the extended transition state (ETS)[13,25] scheme with the natural orbitals for the chemical valence (NOCV)[26] method (namely ETS-NOCV scheme) is introduced to metallic complexes as well as organic molecules, offering a compact picture of chemical bond formation and its different components, as well as donor–acceptor properties in the molecular complex.[2,27–29] In the combined ETS-NOCV scheme, the orbital interaction energy (ΔE_{orb}) between reacting fragments is expressed in terms of NOCV eigenvalues (ν_k) as

$$\Delta E_{orb} = \sum_k \Delta E_{orb}{}^k = \sum_{k=1}^{M/2} \nu_k \left[-F_{-k,-k}^{TS} + F_{k,k}^{TS} \right]$$

Where $F_{-k,-k}^{TS}$ and $F_{k,k}^{TS}$ are the diagonal Kohn–Sham matrix elements defined over NOCV with respect to the transition state (TS) density (at the midpoint between density of molecule and the sum of fragment densities). Each complementary NOCV pair represents one of the charge deformations $\Delta\rho_k$. The abovementioned components $\Delta E_{orb}{}^k$ provide energetic estimation of $\Delta\rho_k$ that may be related to the importance of a particular electron flow channel for the bonding between considered molecular fragments.[27b,c]

Understanding the properties of the metal–ligand chemical bond is important for rationalizing and predicting the catalytic performance of N,N'-dioxide–metal complexes and developing new catalysts. To date, only few studies have been reported on the electronic properties of a chelating multidentate ligand as compared to those on mono or bidentate phosphines.[14b,30,31] The ranking of the donor ability of the chiral N,N'-dioxide ligand featuring four coordinating end groups still remains a challenge. In our previous calculations,[3a,b] we studied the influence of the chiral backbone, linkage, and the substituent of aniline in the N,N'-dioxide–Mg(II) catalyst on its reactivity towards a dicarbonyl compound (isatin) and the corresponding chiral inductivity in asymmetric carbonyl–ene reaction. Herein, we changed the substituent of amide in the ligand in the N,N'-dioxide–Sc(III) catalysts to investigate the catalytic behaviour of these catalysts towards three mono-carbonyl compounds
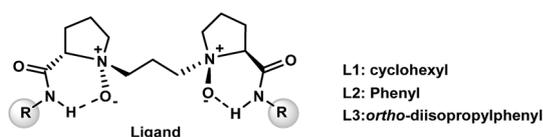
(formaldehyde, benzaldehyde, and chalcone) *via* analysis of the donor–acceptor interaction (Scheme 1). Furthermore, the influence of the counterion from two scandium reagents ($Sc(OTf)_3$ and $Sc(OiPr)_3$) on substrate–catalyst interaction (catalytic abilities) has been explored by the DFT method.

Computational details

Geometry optimization and frequency calculations are performed *via* density functionary theory (DFT) using the Gaussian 09 program package.[32] The M06 hybrid functional[33] is adopted, in conjugation with the 6-31+G** basis set.[34] Natural bond orbital (NBO)[35] analysis is employed to obtain further insight into the electronic properties of the system at the same theoretical level. The results of the activation strain model (ASM) on hexacoordinate chiral N,N'-dioxide–Sc(III) complexes are shown in Tables S1–S3,† in which the reaction energy ΔE_r between metal-based fragment and ligand or carbonyl substrate in the complexes is decomposed into two chemical meaningful components: the distortion energy (ΔE_{strain}) and interaction energy (ΔE_{int}), by Gaussian 09. To understand the factors influencing the donor–acceptor interaction, ΔE_{int} is further decomposed into electrostatic interaction (ΔV_{elstat}), Pauli repulsion (ΔE_{Pauli}), and orbital interaction (ΔE_{oi}) (*i.e.*, $\Delta E_{int} = \Delta V_{elstat} + \Delta E_{Pauli} + \Delta E_{oi}$) by energy decomposition analysis (EDA). EDA and ETS-NOCV calculations are performed by single-point calculation based on the optimized geometries obtained by Gaussian 09 using the Amsterdam density functional (ADF) program[36] at the M06/TZP level. We selected $ScCl_3$ and $Sc(OTf)_3$ compounds as models to examine the multi-reference character of scandium compounds at the CCSD/6-31+G**//M06/6-31+G** level using the Gaussian 09 program. The corresponding T1 diagnostics are predicted to be 0.016 for $ScCl_3$ and 0.018 for $Sc(OTf)_3$, which are smaller than the criteria 0.02, as suggested by Lee and Taylor.[37]

Results and discussion

Donor–acceptor interaction between the ligand and $[Sc(OTf)]^{2+}$ species

Herein, we studied three Sc(III)-complexes (L–$[Sc(OTf)]^{2+}$) formed by the coordination of N,N'-dioxide ligand (L1–L3) to $[Sc(OTf)]^{2+}$ in the gas phase. The corresponding complexes are denoted as L1–Sc(III)–OTf, L2–Sc(III)–OTf, and L3–Sc(III)–OTf for convenience. The coordination processes are exothermic by −275.8 to −290.8 kcal mol^{-1}. As shown in Fig. S1,† the main structural parameters of these three complexes are similar, with the average distances between the four O-donors in the ligands to the Sc cation of 2.066–2.075 Å. NBO analysis indicates that the charge transfer (CT) from ligand to the $[Sc(OTf)]^{2+}$ moiety exhibits the following trend: L1–Sc(III)–OTf (0.942) > L2–Sc(III)–OTf (0.923) > L3–Sc(III)–OTf (0.913). As a result, the natural population analysis (NPA) of charge accumulated on the Sc(III) centre in L3–Sc(III)–OTf (1.629) is slightly larger than those of L1–Sc(III)–OTf (1.600) and L2–Sc(III)–OTf (1.622). As shown in Table 1, the bonding energy (ΔE_{BE}) for L1–Sc(III)–OTf with an aliphatic cyclohexyl group is higher than those of the complexes

L1: cyclohexyl
L2: Phenyl
L3: *ortho*-diisopropylphenyl

Ligand

Scheme 1 Three L-proline-derived chiral N,N'-dioxide ligands (L1–L3).

Table 1 Results of NBO and ETS–NOCV calculations for hexacoordinate complexes formed by ligand (L1–L3) with $[Sc(OTf)]^{2+}$ fragments. The energies are in kcal mol^{-1}

Complex	Charge[a]	CT[b]	ΔE_{Pauli}	ΔV_{elstat}	ΔE_{oi}	ΔE_{orb}^{σ} (1)	ΔE_{orb}^{σ} (2)	ΔE_{BE}[c]
L1–Sc(III)–OTf	1.600	0.942	165.0	−284.4	−283.8	−74.8	−97.1	−403.2
L2–Sc(III)–OTf	1.622	0.923	163.8	−272.1	−284.0	−73.4	−100.4	−392.3
L3–Sc(III)–OTf	1.629	0.913	165.3	−273.1	−292.7	−71.8	−96.0	−400.6

[a] NPA charge accumulated on Sc(III) ion in the hexacoordinate complexes. [b] Charge transfer (CT) from the ligand (L1–L3) to the $[Sc(OTf)]^{2+}$ fragment. [c] Bonding energy (BE) between the ligand and the $[Sc(OTf)]^{2+}$ fragment obtained by ADF calculation.

containing aromatic substituent ligands (L2 and L3). These results indicate that there exists a strong interaction between L1 and $[Sc(OTf)]^{2+}$ fragment.

$\Delta \rho(1)$
$\Delta E_{orb}^{\sigma}(1) = -74.8$ kcal mol^{-1}

$\Delta \rho(2)$
$\Delta E_{orb}^{\sigma}(2) = -97.1$ kcal mol^{-1}

(a)

$\Delta \rho(1)$
$\Delta E_{orb}^{\sigma}(1) = -73.4$ kcal mol^{-1}

$\Delta \rho(2)$
$\Delta E_{orb}^{\sigma}(2) = -100.4$ kcal mol^{-1}

(b)

$\Delta \rho(1)$
$\Delta E_{orb}^{\sigma}(1) = -71.8$ kcal mol^{-1}

$\Delta \rho(2)$
$\Delta E_{orb}^{\sigma}(2) = -96.0$ kcal mol^{-1}
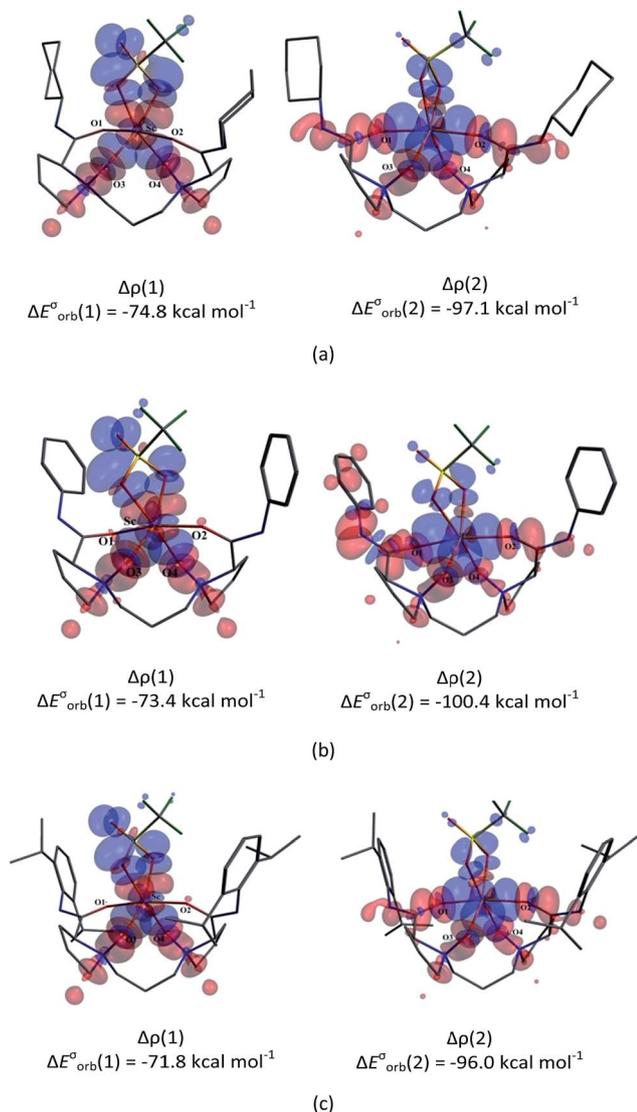
(c)

Fig. 1 Dominating contributions to the deformation density $\Delta \rho$ associated with the coordination interaction between the ligand L1 and the $[Sc(OTf)]^{2+}$ fragment in L1–Sc(III)–OTf (a), L2–Sc(III)–OTf (b), and L3–Sc(III)–OTf (c) complexes determined by the ETS–NOCV analysis. The contour value is $|\Delta \rho| = 0.001$ au. The blue/red contours correspond to accumulation/depletion of electron density.

EDA analysis suggests that the electrostatic and orbital interactions are the main contributors for ligand–$[Sc(OTf)]^{2+}$ interactions in these three complexes. For L1–Sc(III)–OTf, the electron-donating cyclohexyl group enhances the electrostatic interaction between L1 and $[Sc(OTf)]^{2+}$ fragments ($\Delta V_{elstat} = -284.4$ kcal mol^{-1}), contributing to a more stabilizing interaction energy. For L2–Sc(III)–OTf and L3–Sc(III)–OTf, the ΔV_{elstat} are comparable (−272.1 vs. −273.1 kcal mol^{-1}). Although introduction of ortho-iPr groups into L3 slightly increases the destabilizing ΔE_{Pauli} (165.3 kcal mol^{-1}) in L3–Sc(III)–OTf, the more stabilizing orbital interaction ($\Delta E_{oi} = 292.7$ kcal mol^{-1}) compensates for this unfavourable Pauli repulsion. Consequently, the ΔE_{BE} for L3–Sc(III)–OTf is 8.3 kcal mol^{-1}, more stable than that for L2–Sc(III)–OTf.

To quantify the electron-transfer process between ligand and $[Sc(OTf)]^{2+}$ moieties in these complexes, we visualized the deformation density ($\Delta \rho$), and the corresponding orbital energies are shown in Fig. 1. $\Delta \rho$ (1) represents the σ-donation from the N-oxide units of the ligand to the unoccupied $d_{x_2-y_2}$ orbital of the Sc(III) centre, with ΔE_{orb}^{σ} (1) of −71.8 to −74.8 kcal mol^{-1}. For $\Delta \rho$ (2), the electronic density accumulation appears in the coordination region between four O-donors and metal-fragments, thus indicating an electron flow from the ligand to the metal ion to strengthen O–Sc bonding. Interestingly, these effects also weaken the interaction between the counter OTf ion and metal centre, accompanying electronic density flow back from Sc(III) ion to OTf anion. This cooperation effect of coordination units in the chiral N,N′-dioxide–metal complex has also been observed in our previous study.[3a]

Effect of ligand in the Sc(III)-complex on the activation of CH$_2$O

The hexacoordinate complexes (L1–CH$_2$O–OTf, L2–CH$_2$O–OTf, and L3–CH$_2$O–OTf) formed by coordinating formaldehyde (CH$_2$O) to an L–$[Sc(OTf)]^{2+}$ complex were then investigated. Herein, the counter OTf anion occupies one coordinating site to stabilize the corresponding octahedral geometries (Fig. 2). Compared to free CH$_2$O, the C=O bonds in these complexes are lengthened by 0.021–0.026 Å. Moreover, the corresponding Wiberg bond indices (WBI) decrease from 1.912 to 1.635–1.654. These results suggest that the C=O bonds of CH$_2$O in Lm–CH$_2$O–OTf (m = 1–3) are significantly weakened. The NBO analysis indicates that the charge transfer (CT) occurs from CH$_2$O to a catalyst accompanying the coordination process; this leads to electronic density re-distribution in the CH$_2$O moiety.
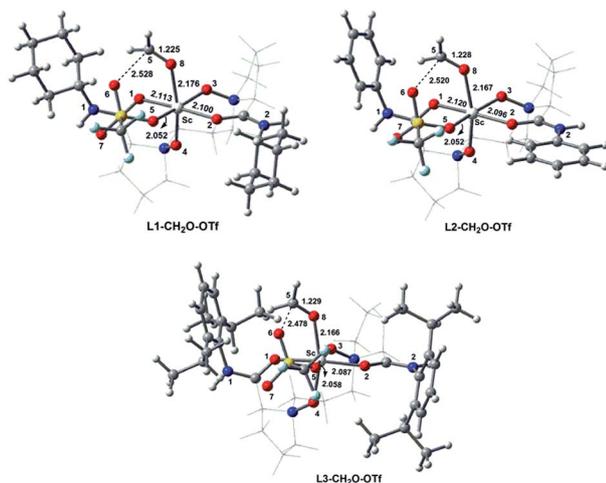
Fig. 2 Optimized geometries of the three hexacoordinate complexes L1–CH$_2$O–OTf, L2–CH$_2$O–OTf, and L3–CH$_2$O–OTf. Selected bond lengths are in Å. The chiral backbone in ligands is shown in grey colour for clarity.

Consequently, the C=O bond becomes more polarized with an increase in dipole moment (from 2.533 Debye in free CH$_2$O to 2.660–2.644 Debye). Accordingly, the C=O stretching vibration frequency ($\nu_{C=O}$, cm^{-1}) red-shifts from 1864 cm^{-1} in free CH$_2$O to 1747–1765 cm^{-1} in the complexes. For L3–CH$_2$O–OTf, the WBI of C=O bond is smaller than those of L1–CH$_2$O–OTf and L2–CH$_2$O–OTf. Moreover, the more negative charge accumulates on the O8 atom (−0.652 vs. −0.621 for L1–CH$_2$O–OTf and −0.630 for L2–CH$_2$O–OTf), which is consistent with the stronger polarity character of the C=O bond and lower $\nu_{C=O}$ (1765 cm^{-1}) in the CH$_2$O moiety. These results indicate that the catalyst with the L3 ligand exhibits slightly superior reactivity towards the CH$_2$O substrate.

Starting from the optimized structures of the three complexes, we performed the relaxed potential energy surface (PES) scan by increasing the distance between CH$_2$O and Sc(III) centre ($R_{O8\cdots Sc}$, Å) by 0.05 Å at the M06/6-31+G** level. The variation of abovementioned electronic descriptors are shown in Tables S1–S3.† As shown in Fig. 3a and b, $\nu_{C=O}$ and the corresponding WBI for the C5=O8 bond exhibit an increasing tendency with $R_{O8\cdots Sc}$. The corresponding correlation equations are shown in Table 2, with R^2 of 0.991–0.997 and 0.999. Although the WBI of the C=O bond of the CH$_2$O moiety in L1–CH$_2$O–OTf and L2–CH$_2$O–OTf is comparable (1.654 vs. 1.640), the C=O bond in L2–CH$_2$O–OTf becomes remarkably less polarized upon lengthening the O8···Sc distance. As a result, a steeper variation of $\nu_{C=O}$ is observed for L2–CH$_2$O–OTf (Fig. 3a). Different from $\nu_{C=O}$, the WBI of O8···Sc interaction decreases linearly as the distance between CH$_2$O and catalyst increases (Fig. 3b). Good linear correlations are observed for the three complexes, with an R^2 of 0.995–0.997 (Table 3).

Activation strain model (ASM) analysis indicates that the interaction energy term ΔE_{int} makes a major contributions to the CH$_2$O–L–[Sc(OTf)]$^{2+}$ interaction in the three abovementioned complexes as compared to the deformation energy
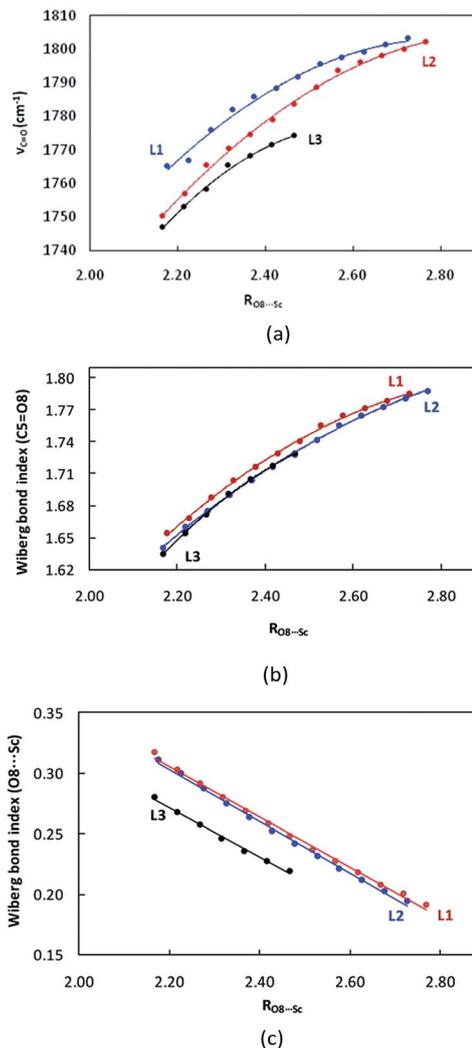

Fig. 3 Variation of the C=O stretching vibration frequency ($\nu_{C=O}$, cm^{-1}) (a), the corresponding Wiberg bond index (WBI) of the C=O bond (b), and WBI of the O8···Sc interaction (c) in L1–CH$_2$O–OTf, L2–CH$_2$O–OTf, and L3–CH$_2$O–OTf complexes with the increasing distance between O8 and Sc(III) ($R_{O8\cdots Sc}$, Å).

ΔE_{strain}. Furthermore, the deformation energies of the metal-fragment ($\Delta E_{strain(CAT)}$) are significantly more destabilizing than that of the CH$_2$O fragment ($\Delta E_{strain(CH_2O)}$). Similarly, there also exist good correlations between $R_{O8\cdots Sc}$ and ΔE_{int}, with the coefficient of 0.997–0.999 (Fig. 4). Compared to that in L1–CH$_2$O–OTf and L2–CH$_2$O–OTf, ΔE_{int} in L3–CH$_2$O–OTf is clearly more stabilizing at any given point along the O8···Sc distance; this indicates the stronger donor–acceptor interaction between CH$_2$O and L3–[Sc(OTf)]$^{2+}$ moiety, as well as Lewis acidity of Sc(III) ion in L3–CH$_2$O–OTf. These results are in good agreement with a larger electron-deficient character for the Sc(III) centre in L3–CH$_2$O–OTf (NPA charge accumulated on Sc(III) cation is 1.647). Although the *ortho*-iPr groups in ligand L3 increase the Pauli repulsion between CH$_2$O and Sc-fragment (ΔE_{Pauli} = 40.1 kcal mol^{-1}), the more stabilizing energies (electrostatic interaction ΔV_{elstat} and orbital interaction ΔE_{oi}) compensates for this destabilizing steric repulsion; this leads to a more

Table 2 Correlations between $\nu_{C=O}$ (cm^{-1}), Wiberg bond index (WBI) of C=O bond in the CH$_2$O moiety, the O8···Sc interaction as well as ΔE_{int} (kcal mol^{-1}) with O8···Sc distance ($R_{O8···Sc}$ Å) for L1–CH$_2$O–OTf, L2–CH$_2$O–OTf, and L3–CH$_2$O–OTf complexes

Ligand	N^a	Equations	R^2
L1	12	$\nu_{C=O} = -96.9 \times (R_{O8···Sc})^2 + 544.9 \times (R_{O8···Sc}) + 1037.4$	0.991
		$WBI_{C5=O8} = -0.227 \times (R_{O8···Sc})^2 + 1.357 \times (R_{O8···Sc}) - 0.224$	0.999
		$WBI_{O8···Sc} = -0.214 \times (R_{O8···Sc}) + 0.774$	0.997
		$\Delta E_{int} = 11.6 \times (R_{O8···Sc})^2 - 34.4 \times (R_{O8···Sc}) - 19.6$	0.997
L2	13	$\nu_{C=O} = -91.5 \times (R_{O8···Sc})^2 + 537.3 \times (R_{O8···Sc}) + 1015.0$	0.997
		$WBI_{C5=O8} = -0.170 \times (R_{O8···Sc})^2 + 1.085 \times (R_{O8···Sc}) + 0.091$	0.999
		$WBI_{O8···Sc} = -0.212 \times (R_{O8···Sc}) + 0.770$	0.997
		$\Delta E_{int} = 9.2 \times (R_{O8···Sc})^2 - 21.6 \times (R_{O8···Sc}) - 39.4$	0.998
L3	7	$\nu_{C=O} = -161.7 \times (R_{O8···Sc})^2 + 841.1 \times (R_{O8···Sc}) + 683.4$	0.995
		$WBI_{C5=O8} = -0.355 \times (R_{O8···Sc})^2 + 1.958 \times (R_{O8···Sc}) - 0.942$	0.999
		$WBI_{O8···Sc} = -0.204 \times (R_{O8···Sc}) + 0.720$	0.995
		$\Delta E_{int} = 21.7 \times (R_{O8···Sc})^2 - 80.0 \times (R_{O8···Sc}) + 27.5$	0.999

^{a} Number of data points employed in the correlation.

Table 3 Results of ASM, EDA, and ETS-NOCV calculations for hexacoordinate complexes. The energies are in kcal mol^{-1}

					ΔE_{strain}								
Ligand	Substituent	Counterion	Carbonyl substrate	ΔE_{int}^a	CAT	Carbonyl substrate	Sum	ΔE_r	ΔE_{Pauli}	ΔV_{elstat}	ΔE_{oi}	ΔE_{orb} (1)	ΔE_{orb} (2)
L1	Cyclohexyl	OTf	CH$_2$O	−39.0(−37.0)	14.4	0.7	15.0	−24.0	37.1	−43.6	−30.5	−31.5	−15.6
L2	Ph	OTf	CH$_2$O	−42.4(−40.8)	15.0	0.8	15.8	−26.6	39.6	−46.6	−33.8	−34.5	−16.8
L3	2,6-iPr	OTf	CH$_2$O	−43.6(−41.1)	19.1	0.8	20.0	−23.6	40.1	−47.3	−33.9	−34.1	−18.2
L3	2,6-iPr	OiPr	CH$_2$O	−32.6(−30.9)	2.3	0.3	2.6	−30.0	22.3	−34.3	−18.9	−25.7	−3.3
L3	2,6-iPr	OTf	PhCHO	−56.4(−53.1)	20.0	2.0	22.0	−34.4	42.7	−56.8	−39.0	−34.4	−21.6
L3	2,6-iPr	OTf	Chalcone	−71.7(−67.0)	21.7	4.6	26.3	−45.4	47.7	−65.7	−49.0	−33.5	−27.0

^{a} Interaction energies obtained by ADF are shown in bracket.

stabilizing ΔE_{int} (−41.1 kcal mol^{-1}). Compared to the case of L3–Sc(III)–OTf, the orbital interaction ΔE_{oi} between the CH$_2$O-fragment and Sc(III)-fragment is smaller than electrostatic energy ΔV_{elstat} by 13.4 kcal mol^{-1} (−33.9 vs. −47.3 kcal mol^{-1}) in L3–CH$_2$O–OTf. Therefore, the electrostatic interaction is the major driving force to form L3–CH$_2$O–OTf by interaction between CH$_2$O and L3–[Sc(OTf)]$^{2+}$ moiety.

For L1, the electron-donating cyclohexyl groups in the amide units enhance the electronic density transfer from the ligand to

the Sc(III) center in the L1–CH$_2$O–OTf complex; this decreases the Lewis acidity of metal ion ($\Delta E_{int} = -37.0$ kcal mol^{-1}). As expected, both ΔV_{elstat} and ΔE_{oi} are less stabilizing than those in L3–CH$_2$O–OTf by 3.7 and 3.4 kcal mol^{-1}, respectively. With respect to L2, the phenyl group on the right brachial amide tends to be placed in the same plane to the carbonyl of amines in L2–CH$_2$O–OTf. A good conjugate effect between the phenyl group and carbonyl of amines compensates for the electronic-deficient character of Sc(III) cation in L2–CH$_2$O–OTf by strengthening the electron density transfer from ligand to metal, decreasing the stabilizing attracting term (ΔV_{elstat} and ΔE_{oi}) between CH$_2$O-fragment and Sc(III)-fragment by 1.5 kcal mol^{-1}. As a result, the ΔE_{int} of L2–CH$_2$O–OTf is less stabilizing than that of L3–CH$_2$O–OTf (−40.8 vs. −41.1 kcal mol^{-1}).

We visualized the deformation density associated with the orbital interaction between CH$_2$O and the Sc(III)-based fragments in the three complexes. The two dominating components of deformation density, $\Delta\rho$ (1) and $\Delta\rho$ (2), with the corresponding energy values are presented in Fig. 5 and S3.† As shown in Fig. 5, the accumulation of electron density appears in the region between the O8 atom and the scandium centre in L3–CH$_2$O–OTf; this indicates electrons flowing from σ-donor O lone electron pair of CH$_2$O to unoccupied d orbital of Sc(III) ion
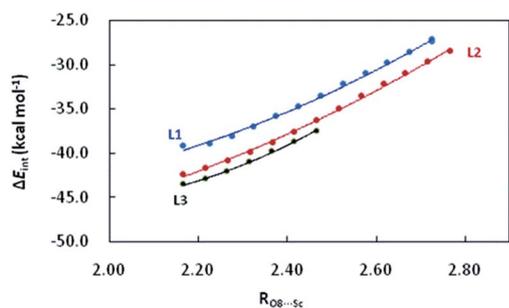

Fig. 4 Variation of the interaction energy ΔE_{int} (kcal mol^{-1}) between CH$_2$O and L–[Sc(OTf)]$^{2+}$ moiety with the increasing distance between O8 and Sc(III) ($R_{O8···Sc}$, Å) in L1–CH$_2$O–OTf, L2–CH$_2$O–OTf, and L3–CH$_2$O–OTf complexes.

$\Delta\rho(1)$
$\Delta E_{orb}(1) = -34.1$ kcal mol^{-1}

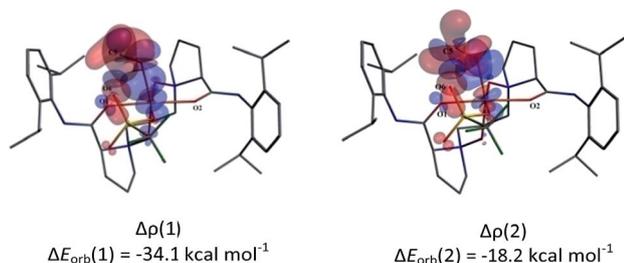$\Delta\rho(2)$
$\Delta E_{orb}(2) = -18.2$ kcal mol^{-1}

Fig. 5 Dominating contributions to the deformation density $\Delta\rho$ describing the coordination interaction between CH_2O and scandium-based fragments for L3–CH_2O–OTf complex by ETS-NOCV analysis. The contour value is $|\Delta\rho| = 0.001$ au. The blue/red contours correspond to accumulation/depletion of electron density.

to form the Sc–O bond. Simultaneously, the depletion of electron density on π double C=O bond of CH_2O suggests the weakening of π bonds in CH_2O. With respect to the second NOCV-based deformation density contribution $\Delta\rho$ (2), it presents 36% of the interfragment orbital interaction, accompanying the weakening of C–H as well as C=O bonds in CH_2O. In addition, the slight electronic density accumulation between the O6 atom of OTf anion and the C8 atom of CH_2O stabilizes the hexacoordinate complexes, further favouring the activation of CH_2O. Similar results are obtained for L1–CH_2O–OTf and L2–CH_2O–OTf, as shown in Fig. S3 in the ESI.†

As shown in Table S4 and Fig. S4 in the ESI,† CDA analysis indicates that the main molecular orbital involving the donor–acceptor interaction and electronic density transfer between CH_2O and L3–Sc(III) in the L3–CH_2O–OTf complex is the occupied HOMO-146 orbital. It is constructed from the HOFO-5 of CH_2O fragment and LUFO-2, LUFO-3, and LUFO-6 orbitals of the L3–Sc(III) fragment. The HOFO-5 is the hybridized orbital of $\sigma(CH_2)$ and s atomic orbital of CH_2O. The total contribution of LUFO orbitals in the L3–Sc(III) fragment is smaller than that of the HOFO-5 of CH_2O moiety by 53.2% (66.4% *vs.* 13.2%). Interestingly, the contribution of the unoccupied orbital in the Sc(III)-based fragment decreases in the order of L3 > L2 > L1, which is in good agreement with electron density transfer from CH_2O to catalysts. Thus, the combination of stronger electrostatic interactions and the more stabilizing orbital interaction contributes to the superior reactivity of L3–[Sc(OTf)]$^{2+}$ towards CH_2O.

Effect of counterion on the activation of CH_2O

To understand the effect of counterion in the catalyst on Lewis acidity of the metal ion as well as the activation of carbonyl, we replaced the OTf anion in L3–CH_2O–OTf with *iso*-propoxy ion (O*i*Pr). The corresponding optimized geometries of the hexacoordinate complexes L3–CH_2O–O*i*Pr are shown Fig. 6. Compared to those for L3–CH_2O–OTf, the O8···Sc distances are longer by 0.094 Å for L3–CH_2O–O*i*Pr. Furthermore, the C=O bond length of CH_2O follows the order L3–CH_2O–OTf > L3–CH_2O–O*i*Pr. This result indicates that CH_2O becomes less weakened in L3–CH_2O–O*i*Pr. The O5–Sc distance in L3–CH_2O–O*i*Pr is shorter significantly than those of L3–CH_2O–OTf (1.862 Å *vs.* 2.058 Å); this indicates a stronger interaction between O*i*Pr and Sc(III) centre. This result could be attributed to the stronger basicity of O*i*Pr anion than that of OTf anion. Suffering large steric repulsion from O*i*Pr, tetradentate N,N'-dioxide ligand moves slightly far away from the metal centre. Accordingly, the average O–Sc distance in ligand in L3–CH_2O–O*i*Pr is as long as 2.131 Å. This effect also weakens the coordinate interaction of CH_2O to Sc(III) ion; this leads to the less stabilizing ΔV_{elstat} (−34.3 kcal mol^{-1}) and ΔE_{oi} (−18.9 kcal mol^{-1}). NBO analysis indicate that the energy level of LUMO orbitals in two complexes has the order of L3–CH_2O–O*i*Pr > L3–CH_2O–OTf. Accordingly, the electrophilic indices ω of complexes are 9.4 eV for L3–Sc(III)–OTf and 8.1 eV for L3–Sc(III)–O*i*Pr. Similar to the case of L3–CH_2O–OTf, the ΔV_{elstat} is still a major contributor in L3–CH_2O–O*i*Pr, which is also confirmed by AIM analysis (Fig. 6). The positive Laplacian of electronic density $\nabla^2\rho$ at $(3, -1)$ bonding critical points (a and b) is observed between CH_2O or O*i*Pr ion to metal centre, which is similar to that of L3–CH_2O–OTf in Fig. S5.† Furthermore, ΔE_{int} exhibits the following order L3–CH_2O–OTf > L3–CH_2O–O*i*Pr, which is in good agreement with the abovementioned results of electrophilic indices. The inferior reactivity of the catalyst with Sc(O*i*Pr)$_3$ as a precursor was also observed in the experiments.[3d] Therefore, the counter ion could adjust the electrophilicity of the Sc(III)-complex by affecting ΔV_{elstat} and ΔE_{oi}. The Lewis acidity of Sc(III) ion in L3–CH_2O–OTf is stronger than that of L3–CH_2O–O*i*Pr, consequently, exhibiting high reactivity towards the nucleophilic CH_2O substrate.

Variation of the carbonyl substrate

We used two more carbonyl substrates (PhCHO and chalcone) to further evaluate the reactivity of L3–[Sc(OTf)]$^{2+}$. The
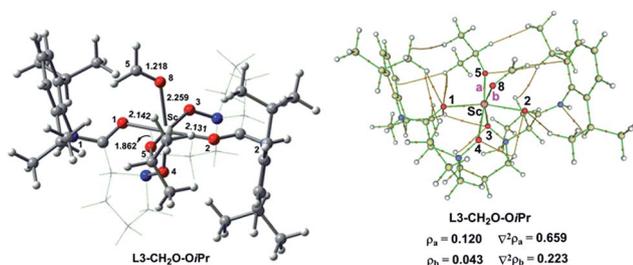

Fig. 6 Optimized geometry and AIM analysis of hexacoordinate L3–CH_2O–O*i*Pr. Selected bond lengths are in Å. The chiral backbone in the ligand is shown in grey colour for clarity.
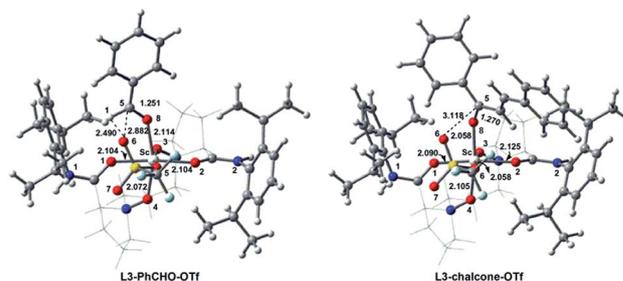

Fig. 7 Optimized geometries of the hexacoordinate complexes L3–PhCHO–OTf and L3–chalcone–OTf. Selected bond lengths are in Å. The chiral backbone in ligands is shown in grey colour for clarity.

optimized geometries for the hexacoordinate complexes L3–PhCHO–OTf and L3–chalcone–OTf are shown in Fig. 7. As shown in Table S5,† NBO analysis indicates that more negative charges accumulated on the O atom of free PhCHO or chalcone substrates because of electron delocalization of the adjacent phenyl ring (−0.561 and −0.597 *vs.* −0.533 in CH_2O). Consequently, the nucleophilicity of PhCHO and chalcone is significantly enhanced to 2.02 and 2.81 eV, respectively, as compared to that of CH_2O (1.73 eV). This effect favours the coordination interaction between PhCHO or chalcone and Sc(III) centre, with shorter O8···Sc distances of 2.114 Å for L3–PhCHO–OTf and 2.058 Å for L3–chalcone–OTf, respectively. EDA analysis indicates that the interaction energies ΔE_{int} between carbonyl substrates and scandium-based fragment are −53.1 kcal mol^{-1} for L3–PhCHO–OTf and −67.0 kcal mol^{-1} for L3–chalcone–OTf, which are more stabilizing than that of L3–CH_2O–OTf (−41.1 kcal mol^{-1}, Table S3†). Furthermore, the NOCV deformation density as well as the corresponding energy $\Delta E_{orb}^{\sigma} = \Delta E_{orb}$ (1) + ΔE_{orb} (2) for L3–PhCHO–OTf and L3–chalcone–OTf complexes are higher than that of L3–CH_2O–OTf (56.0 and 60.5 kcal mol^{-1} *vs.* 52.3 kcal mol^{-1}). These results indicate that L3–[Sc(OTf)]$^{2+}$ exhibits higher reactivity for PhCHO and chalcone substrates as compared to that for CH_2O. Contrary to PhCHO, the chalcone with a more significant π-conjugated structure tends to coordinate to L3–[Sc(OTf)]$^{2+}$, with most stabilizing ΔV_{elstat} (−65.7 kcal mol^{-1}) and ΔE_{oi} (−49.0 kcal mol^{-1}) for carbonyl–Sc(III)–fragment interaction. The C=O bonds of PhCHO and chalcone in these complexes are lengthened by 0.039 and 0.044 Å, with $\Delta \nu_{C=O}$ of 149.3 and 200.5 cm^{-1}, respectively, indicating that C=O bonds are activated significantly in L3–PhCH$_2$O–OTf and L3–chalcone–OTf. These results are in good agreement with the excellent reactivity of chiral N,N′-dioxide–Sc(III) catalysts for the transformation of chalcone or PhCHO substrates in organometallic catalysis.[1a,b]

Conclusions

Theoretical investigation on donor–acceptor interaction between a ligand and carbonyl compound with a metal ion in N,N′-dioxide–Sc(III) complex is performed using the DFT method. The effect of the substituent of the ligand and counter ion on Lewis acidity as well as the reactivity of the Sc(III)-complex towards carbonyl compound is studied. These calculations reveal the following conclusions:

(1) The orbital attraction is the major contributor to the interaction between the chiral N,N′-dioxide ligand and Sc(III)-based fragment in the L–[Sc(OTf)]$^{2+}$ complex. The ligand with the cyclohexyl group in amide exhibits a stronger coordination ability towards the Sc(III) centre as compared to the ligands with an aromatic ring.

(2) The electrostatic interaction is the major driving force to form a hexacoordinate complex by interaction between CH_2O and L3–[Sc(OTf)]$^{2+}$ moiety. Variation of amide moiety in substituents of the ligands adjusts electrostatic energy as well as orbital energy between CH_2O and L–[Sc(OTf)]$^{2+}$ fragment in hexacoordinate complexes, affecting the activation of carbonyl compound. The combination of stronger ΔV_{elstat} and more stabilizing ΔE_{oi} contributes to the high catalytic performance of complex with a 2,6-diisopropylphenyl group towards CH_2O.

(3) The counter anion in the complex tunes the energy level of the LUMO orbital of N,N′-dioxide–Sc(III) complex; this affects the electrophilicity of the L–Sc(III)-complex towards the carbonyl substrate. The Lewis acidity of the metal ion in the complex could be adjusted by changing Pauli repulsion, electrostatic, as well as orbital interaction between the carbonyl compound and metal centre.

(4) PhCHO and chalcone with high nucleophilicity exhibit excellent reactivity in the presence of L–[Sc(OTf)]$^{2+}$ complex; this may be related to more stabilizing electrostatic and orbital interaction. The activation process accompanies with more significantly electron density transfer from a carbonyl compound to a Sc-based fragment.

Conflicts of interest

There are no conflicts of interest to declare.

Acknowledgements

Notes and references

1 (a) X. H. Liu, L. L. Lin and X. M. Feng, *Acc. Chem. Res.*, 2011, **44**, 574; (b) X. H. Liu, L. L. Lin and X. M. Feng, *Org. Chem. Front.*, 2014, **1**, 298; (c) K. Shen, X. H. Liu, L. L. Lin and X. M. Feng, *Chem. Sci.*, 2012, **3**, 327; (d) X. H. Liu, H. F. Zheng, Y. Xia, L. L. Lin and X. M. Feng, *Acc. Chem. Res.*, 2017, **50**, 2621.

2 M. Fusè, I. Rimoldi, E. Cesarotti, S. Rampino and V. Barone, *Phys. Chem. Chem. Phys.*, 2017, **19**, 9028.

3 (a) J. M. Wang, Z. S. Su, N. Yang and C. W. Hu, *J. Org. Chem.*, 2016, **81**, 6444; (b) J. M. Wang, Y. N. Zuo, C. W. Hu and Z. S. Su, *Catal. Sci. Technol.*, 2017, 7, 2183; (c) Y. N. Zuo, Z. S. Su, J. M. Wang and C. W. Hu, *Catal. Today*, 2017, **298**, 130–137; (d) Q. Zhang, X. Xiao, L. L. Lin, X. H. Liu and X. M. Feng, *Org. Biomol. Chem.*, 2011, **9**, 5748; (e) Y. Y. Chu, X. H. Liu, W. Li, X. L. Hu, L. L. Lin and X. M. Feng, *Chem. Sci.*, 2012, **3**, 1996; (f) M. S. Xie, X. H. Liu, Y. Zhu, X. H. Zhao, Y. Xia, L. Lin and X. M. Feng, *Chem.–Eur. J.*, 2011, **17**, 13800.

4 M. J. S. Dewar, *Bull. Soc. Chim. Fr.*, 1951, **18**, C71–C79.

5 J. Chatt and L. A. Duncanson, *J. Chem. Soc.*, 1953, **3**, 2939.

6 M. Mitoraj and A. Michalak, *Organometallics*, 2007, **26**, 6576.

7 G. Frenking and N. Fröhlich, *Chem. Rev.*, 2000, **100**, 717.

8 S. Dapprich and G. Frenking, *J. Phys. Chem.*, 1995, **99**, 9352.

9 A. W. Ehlers, S. Dapprich, S. F. Vyboishchikov and G. Frenking, *Organometallics*, 1996, **15**, 105.

10 G. Frenking, K. Wichmann, N. Fröhlich, J. Grobe, W. Golla, D. Le Van, B. Krebs and M. Läge, *Organometallics*, 2002, **21**, 2921.

11 V. Tognetti, L. Joubert, P. Cortona and C. Adamo, *J. Phys. Chem. A*, 2009, **113**, 12322.

12 Y. Mo, J. Gao and S. D. Peyerimhoff, *J. Chem. Phys.*, 2000, **112**, 5530.

13 T. Ziegler and A. Rauk, *Inorg. Chem.*, 1979, **18**, 1755.

14 (a) C. A. Tolman, *Chem. Rev.*, 1977, **77**, 313; (b) N. Fey, *Dalton Trans.*, 2010, **39**, 296; (c) S. L. Mukerjee, S. P. Nolan, C. D. Hoff and R. L. Delavega, *Inorg. Chem.*, 1988, **27**, 81; (d) N. Fey, A. G. Orpen and J. N. Harvey, *Coord. Chem. Rev.*, 2009, **253**, 704.

15 (a) C. H. Suresh and N. Koga, *Inorg. Chem.*, 2002, **41**, 1573; (b) O. Kühl, *Coord. Chem. Rev.*, 2005, **249**, 693; (c) D. J. Nelson and S. P. Nolan, *Chem. Soc. Rev.*, 2013, **42**, 6723.

16 (a) F. Cheng, A. L. Hector, W. Levason, G. Reid, M. Webster and W. Zhang, *Inorg. Chem.*, 2010, **49**, 752; (b) Q. Teng and H. V. Huynh, *Inorg. Chem.*, 2014, **53**, 10964; (c) H. V. Huynh, Y. Han, R. Jothibasu and J. A. Yang, *Organometallics*, 2009, **28**, 5395; (d) K. Verlinden, H. Buhl, W. Frank and C. Ganter, *Eur. J. Inorg. Chem.*, 2015, 2416.

17 L. Perrin, E. Clot, O. Eisenstein, J. Loch and R. H. Crabtree, *Inorg. Chem.*, 2001, **40**, 5806.

18 W. J. van Zeist, R. Visser and F. M. Bickelhaupt, *Chem.–Eur. J.*, 2009, **15**, 6112.

19 I. Fernandez and F. M. Bickelhaupt, *Chem. Soc. Rev.*, 2014, **43**, 4953.

20 I. Fernandez, *Phys. Chem. Chem. Phys.*, 2014, **16**, 7662.

21 D. H. Ess and K. N. Houk, *J. Am. Chem. Soc.*, 2007, **129**, 10646.

22 X. Hong, Y. Liang, A. K. Griffith, T. H. Lambert and K. N. Houk, *Chem. Sci.*, 2014, **5**, 471.

23 Y. F. Yang, Y. Liang, F. Liu and K. N. Houk, *J. Am. Chem. Soc.*, 2016, **138**, 1660.

24 M. von Hopffgarten and G. Frenking, *Wiley Interdiscip. Rev.: Comput. Mol. Sci.*, 2012, **2**, 43.

25 T. Ziegler and A. Rauk, *Theor. Chim. Acta*, 1977, **46**, 1.

26 (a) A. Michalak, M. Mitoraj and T. Ziegler, *J. Phys. Chem. A*, 2008, **112**, 1933; (b) A. Michalak, M. Mitoraj and T. Ziegler, *J. Mol. Model.*, 2008, **14**, 681.

27 (a) M. Mitoraj, M. Parafiniuk, M. Srebro, M. Handzlik, A. Buczek and A. Michalak, *J. Mol. Model.*, 2011, **17**, 2337; (b) M. Mitoraj, *J. Phys. Chem. A*, 2011, **115**, 14708; (c) R. Kurczab, M. Mitoraj, A. Michalak and T. Ziegler, *J. Phys. Chem. A*, 2010, **114**, 8581; (d) G. A. Ardizzoia, M. Bea, S. Brenna and B. Therrien, *Eur. J. Inorg. Chem.*, 2016, 3829.

28 M. Hamdaoui, M. Ney, V. Sarda, L. Karmazin, C. Ailly, N. Ieffert, S. Dohm, A. Hansen, S. Grimme and J. P. Djukic, *Organometallics*, 2016, **35**, 2207.

29 M. Mitoraj, A. Michalak and T. Ziegler, *J. Chem. Theory Comput.*, 2009, **5**, 962.

30 Y. Canac and C. Lepetit, *Inorg. Chem.*, 2017, **56**, 667.

31 C. Flener Lovitt, G. Frenk and G. S. Girolami, *Organometallics*, 2012, **31**, 4122.

32 M. J. Frisch, G. W. Trucks, H. B. Schlegel, G. E. Scuseria, M. A. Robb, J. R. Cheeseman, G. Scalmani, V. Barone, B. Mennucci, G. A. Petersson, H. Akatsuji, M. Aricato, X. Li, H. P. Hratchian, A. F. Izmaylov, J. Bloino, G. Zheng, J. L. Sonnenberg, M. Hada, M. Ehara, K. Toyota, R. Fukuda, J. Hasegawa, M. Ishida, T. Nakajima, Y. Honda, O. Kitao, H. Nakai, T. Vreven, J. A. Montgomery, J. J. E. Peralta, F. Ogliaro, M. Bearpark, J. J. Heyd, E. Brothers, K. N. Kudin, V. N. Staroverov, T. Keith, R. Kobayashi, J. Normand, K. Raghavachari, A. Rendell, J. C. Burant, S. S. Iyengar, J. Tomasi, M. Cossi, N. Rega, J. M. Millam, M. Klene, J. E. Knox, J. B. Cross, V. Bakken, C. Adamo, J. Jaramillo, R. Gomperts, R. E. Stratmann, O. Yazyev, A. J. Austin, R. Cammi, C. Pomelli, J. W. Ochterski, R. L. Martin, K. Morokuma, V. G. Zakrzewski, G. A. Voth, P. Salvador, J. J. Dannenberg, S. Dapprich, A. D. Daniels, O. Farkas, J. B. Foresman, J. V. Ortiz, J. Cioslowski and D. J. Fox, *Gaussian 09, revision D.01*, Gaussian, Inc., Wallingford, CT, 2013.

33 Y. Zhao and D. G. Truhlar, *Acc. Chem. Res.*, 2008, **41**, 157.

34 (a) T. Clark, J. Chandrasekhar, G. W. Spitznagel and P. V. R. Schleyer, *J. Comput. Chem.*, 1983, **4**, 294; (b) V. A. Rassolov, J. A. Pople, M. A. Ratner and T. L. Windus, *J. Chem. Phys.*, 1998, **109**, 1223.

35 A. E. Reed, L. A. Curtiss and F. Weinhold, *Chem. Rev.*, 1988, **88**, 899.

36 E. J. Baerends, T. Ziegler, J. Autschbach, D. Bashford, A. Bérces, F. M. Bickelhaupt, C. Bo, P. M. Boerrigter, L. Cavallo, D. P. Chong, L. Deng, R. M. Dickson, D. E. Ellis, M. vanFaassen, L. Fan, T. H. Fischer, C. F. Guerra, M. Franchini, A. Ghysels, A. Giammona, S. J. A. van Gisbergen, A. W. Götz, J. A. Groeneveld, O. V. Gritsenko, M. Grüning, S. Gusarov, F. E. Harris, P. V. D. Hoek, C. R. Jacob, H. Jacobsen, L. Jensen, J. W. Kaminski, G. V. Kessel, F. Kootstra, A. Kovalenko, M. V. Krykunov, E. V. Lenthe, D. A. McCormack, A. Michalak, M. Mitoraj, S. M. Morton, J. Neugebauer, V. P. Nicu, L. Noodleman, V. P. Osinga, S. Patchkovskii, M. Pavanello, P. H. T. Philipsen, D. Post, C. C. Pye, W. Ravenek, J. I. Rodríguez, P. Ros, P. R. T. Schipper, H. V. Schoot, G. Schreckenbach, J. S. Seldenthuis, M. Seth, J. G. Snijders, M. Solà, M. Swart, D. Swerhone, G. T. Velde, P. Vernooijs, L. Versluis, L. Visscher, O. Visser, F. Wang, T. A. Wesolowski, E. M. van Wezenbeek, G. Wiesenekker, S. K. Wolff, T. K. Woo and A. L. Yakovlev, *ADF2016, Theoretical Chemistry*, Vrije Universiteit, Amsterdam, The Netherlands, http://www.scm.com.

37 (a) W. Y. Jiang, N. J. DeYonker and A. K. Wilson, *J. Chem. Theory Comput.*, 2012, **8**, 460; (b) T. J. Lee and P. R. Taylor, *Int. J. Quantum Chem., Quantum Chem. Symp.*, 1989, **S23**, 199.